AGU PUBLICATIONS

Water Resources Research

RESEARCH ARTICLE
10.1002/2016WR019195

# Characterizing the spatial correlation of daily streamflows

A. Betterle[1,2,3], M. Schirmer[1,2], and G. Botter[3]

[1]EAWAG (Swiss Federal Institute of Aquatic Science and Technology), Department of Water Resources and Drinking Water, Dübendorf, Switzerland, [2]Centre of Hydrogeology and Geothermics (CHYN), University of Neuchâtel, Neuchâtel, Switzerland, [3]Department of ICEA and International Center for Hydrology "Dino Tonini", University of Padova, Padua, Italy

**Key Points:**
- Novel analytical expressions for the spatial correlation of discharge are derived using a process-based stochastic formulation
- The method describes how heterogeneity of climate and landscape impact the spatial variability of flow regimes
- The method shows how nested catchments tend to maximize the spatial correlation of flow regimes

**Correspondence to:**
G. Botter,
gianluca.botter@dicea.unipd.it

**Citation:**
Betterle, A., M. Schirmer, and G. Botter (2017), Characterizing the spatial correlation of daily streamflows, *Water Resour. Res.*, *53*, 1646–1663, doi:10.1002/2016WR019195.

Received 11 MAY 2016
Accepted 23 JAN 2017
Accepted article online 28 JAN 2017
Published online 25 FEB 2017

**Abstract** In this study we propose an analytical framework to estimate the spatial correlation of daily flows at two arbitrary locations within a given hydrologic district or river basin. The method builds on the description of the coupled streamflow dynamics at the outlet of two catchments, which are represented as correlated shot noises forced by Poisson rainfall. Novel analytical expressions for the spatial correlation of discharge are derived using a limited number of parameters that encapsulate effective precipitation regime and catchment drainage rates. The method is suited to describe how heterogeneity of climate and landscape features impact the spatial and temporal variability of flow regimes along river systems. The analysis suggests that frequency and intensity of synchronous effective rainfall events in the relevant contributing catchments are the main driver of the spatial correlation of daily discharge, unless the drainage rates of the two catchments differ by almost one order of magnitude. The method also portrays how the topological arrangement of the two outlets along the river network influences the underlying streamflow correlation and shows how nested catchments tend to maximize the spatial correlation of flow regimes. To demonstrate the potential of the tool, the model is tested on a set of 16 catchments belonging to a 120,000 km$^2$ region of the United States. The application evidences satisfactory performance in reproducing the observed spatial correlation of daily streamflows among the study sites ($RMSE < 0.1$). The approach provides a clue for the characterization of water availability in space at seasonal time scale, with implications for water resources assessment, risk prevention, and ecological studies.

**Plain Language Summary** The importance of freshwater is not limited to drinking water. Water is crucial to produce sustainable energy, to support recreational activities along rivers, agriculture and industry, as well as to supply adequate transportation networks. Freshwater environments represent the elective habitat of many plants and fishes, and they contribute significantly to global-scale biodiversity. The understanding of the water cycle, namely: when, where and how much water is available in rivers - is therefore a crucial issue for a sustainable use of water resources. In this study we develop an analytical method to quantify similarities between the daily flows in two arbitrary locations belonging to one or more rivers. This requires to quantify what are the major climatic and landscape characteristics that control rivers flows. Second, it has to be quantified how these features affect similarity (i.e. synchronicity) of flow records at two arbitrary locations. This work represents a tool to improve our ability to quantify water resources in space and time, providing a theoretical basis to develop strategies for a wiser use of water in the era of climate change.

## 1. Introduction

A proper characterization of streamflow patterns in space and time represents a significant scientific challenge with a wide range of implications for human water uses and ecosystem services conservation [*Postel and Richter*, 2003; *Ziv et al.*, 2012; *Hurford and Harou*, 2014; *McGuire et al.*, 2014]. Despite this, relatively few rivers are adequately monitored [*Blöschl et al.*, 2013; *Kiang et al.*, 2013] and improving the density of existing gauging networks is often challenged by technical and economical limitations that include the availability of financial resources and the accessibility of stream reaches. Therefore, in most practical settings, observational data about spatial and temporal patterns of flow regimes may be inadequate for water resources management and for the prediction of risk associated to floods and droughts.

To cope with the absence of dense discharge gauging networks, many different approaches have been proposed in the literature to predict streamflow availability in sparsely gauged or ungauged catchments [see, e.g., *Blöschl et al.*, 2013, and references therein]. Probabilistic models are typically concerned with the

frequency distribution of discharge (PDF) or with the corresponding flow duration curve (FDC), thus disregarding temporal dynamics of flows. Although certain probabilistic approaches [e.g., *Botter et al*., 2008a; *Müller et al*., 2014] entail a physically based mechanistic formulation that facilitates hydrologic prediction in sparsely gauged catchments and under changing climatic conditions [*Doulatyari et al*., 2015; *Müller and Thompson*, 2015], cross-correlations among multiple outlets have never been studied in that framework. On the contrary, spatial patterns of streamflow regimes are usually accounted for in regionalization methods [*Castellarin et al*., 2004, 2007; *Cheng et al*., 2012], which attempt to establish explicit connections among gauged and ungauged sites based on the concept of hydrologic similarity. In particular, geostatistical methods have proven effective in describing spatial patterns of river flows. For example, *Top-Kriging* [*Skøjen et al*., 2006; *Castiglioni*, 2011; *Lahaa*, 2014] is a topological approach for the interpolation of flow-related variables along river networks that explicitly considers the spatial arrangement of catchments. The *Map Correlation Method* [*Archfield and Vogel*, 2010] is another geostatistical approach devoted to the selection of the gauged section that is most correlated with the target ungauged site. Streamflow correlation, in fact, has been proven to be a better indicator than spatial proximity for transferring flow attributes from gauged to ungauged sites.

Spatially explicit numerical rainfall-runoff models [*Zehe and Blöschl*, 2004; *Rigon et al*., 2006; *Kollet and Maxwell*, 2008; *Costa-Cabral et al*., 2008; *Schaefli et al*., 2014] have the potential to provide a detailed characterization of the spatial and temporal patterns of runoff hydrographs by exploiting information about catchment characteristics and relevant climatic features. However, numerical models require intensive calibration and the application to ungauged outlets remains challenging [*Blöschl*, 2006; *Castiglioni et al*., 2010].

Notwithstanding the progresses made in the characterization of flow regimes, the understanding of spatial connections in streamflows is an area where more research is needed [*Sivakumar and Woldemeskel*, 2014]. In this context, exploring the spatial and temporal structure of the streamflows correlation based on simple climate and hydrologic attributes represents an attractive prospect. The correlation of the streamflows is a synthetic statistical descriptor of similarity between synchronous discharge dynamics at arbitrary pairs of outlets. Therefore, it encapsulates the complex effect of heterogeneous climate, geology, and land cover on flow regimes [*Kiang et al*., 2013]. Highly correlated outlets are likely to display similar discharge dynamics (Figure 1), thereby enabling for a more efficient extrapolation of available streamflow records. For example, a proper characterization of the spatial correlation of streamflows supports the prediction of flow statistics in ungauged sections [*Archfield and Vogel*, 2010; *Messinger and Paybins*, 2014] and facilitate the identification of optimal configurations for water infrastructures along river networks. A physically based characterization of discharge correlation could also contribute to improve the reliability of the estimate of long-term streamflow statistics in sites where only short-term records are available (e.g., via record augmentation techniques [*Hirsch*, 1982; *Vogel and Stedinger*, 1985]).

A better understanding of spatial connections in streamflow dynamics could be used to more efficiently expand existing hydrometric gauging networks [*Kiang et al*., 2013]. In fact, predicted streamflow correlations could be exploited to identify locations that are poorly correlated with existing gauging stations and, thus, are best suited to be equipped with new stream gauges. This would eventually support the optimization of geostatistical techniques designed for the spatial interpolation of observed flow attributes along river networks.

Following a stochastic framework, this work aims to provide a physically based analytical characterization of the seasonal correlation coefficient between daily streamflows at the outlet of two arbitrary catchments (nested or disjointed). The steady state, zero lag streamflow correlation is expressed as a function of lumped parameters that embody seasonal climatic and landscape features (rainfall, soil, vegetation, recession rate) in the contributing areas.

The remainder of this manuscript is organized as follows: section 2 describes the stochastic approach used to derive a general analytical expression for the spatial correlation of daily streamflow. In order to make the general solution operative, some assumptions have to be made about the probability distribution of the effective rainfall depths. For this purpose, a set of alternatives is presented and discussed in section 3, jointly with the derivation of the corresponding analytical expressions of the streamflow spatial correlation. The performances of the model are assessed in section 4, where the model is applied to a set of case studies. A detailed sensitivity analysis is presented in section 5, while the impact of heterogeneity of rainfall, soil, and vegetation properties on the streamflow correlation is further discussed in section 6. A set of conclusions closes the paper.

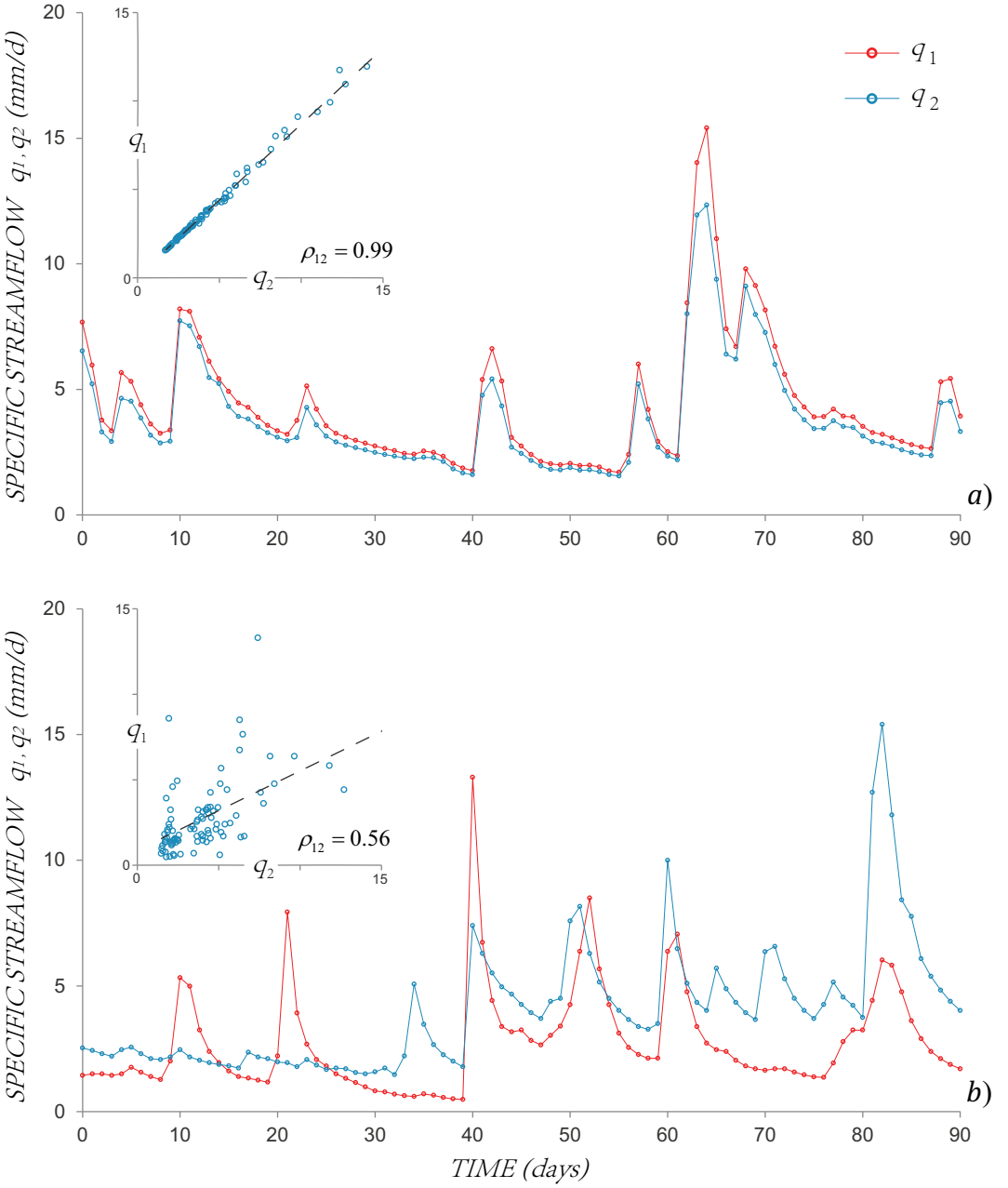


**Figure 1.** Comparison between the daily streamflow time series at two pairs of catchment outlets in the Eastern United States. (a) Little Pigeon River at Sevierville (TN) ($q_1$) and Oconaluftee River at Birdtown (NC) ($q_2$), during autumn; (b) Valley River at Tomotla (NC) ($q_1$) and North Fork Holston River near Gate City (VA) ($q_2$), during spring. The insets show the scatterplots of $q_1$ and $q_2$, and the corresponding cross-correlation. High correlations correspond to similar streamflow dynamics at the two sites.

## 2. Analytical Characterization of Streamflow Correlation: General Framework

In order to develop an analytical expression for the spatial correlation of streamflows at seasonal timescale, we first specify the joint dynamics of daily discharge at two arbitrary catchment outlets during a season. In rivers that are not affected by relevant water storage (e.g., lakes, reservoirs, and snowpacks) abrupt increases of discharge (streamflow jumps) result from the random occurrence of flow-producing (i.e., effective) rainfall events [*Claps et al.*, 2005; *Botter et al.*, 2007a; *Müller et al.*, 2014; *Andres-Domenech et al.*, 2015; *Doulatyari et al.*, 2015]. Each streamflow jump is then followed by a recession resulting from the drainage of the contributing catchment (Figure 1).

The effective rainfall within each catchment is described as a marked Poisson process $\xi_{it}$ with frequency $\lambda_{it}$ (where the subscript $i \in \{1,2\}$ identifies the relevant contributing catchment, and $t$ refers to the "total" series of effective rainfall events). Poisson processes in time describe the occurrence of independent events with exponentially distributed interarrivals [*Kingman*, 1992]. In this case, the marks of the process are represented by the effective rainfalls depths in catchment $i$, $h_i$, that are assumed to be random variables characterized by the probability density function (PDF) $b_{it}$. The frequency of rainfall events is higher than the frequency of runoff producing events because of the ability of the root zone to buffer incoming rainfall during wetting-drying cycles. The buffering capacity of the soil crucially depends on the soil water storage capacity, land cover, and climate [*Milly*, 1994; *Porporato et al*., 2004; *Botter et al*., 2007a; *Botter et al*., 2013; *Thompson et al*., 2011]. The parameters $\lambda_{it}$ hence summarize climate and landscape attributes in the contributing catchments and encapsulate the major nonlinearities in rainfall-runoff transformation.

We also assume that the daily specific discharge (per unit of catchment area) at the considered outlets ($q_1$ and $q_2$) can be expressed as the convolution between the effective rainfall ($\xi_{it}$) and an exponential unit hydrograph

$$\begin{cases} q_1(t) = \int_0^t \xi_{1t}(t-\tau) k_1 \, e^{-k_1 \tau} \, d\tau \\ \\ q_2(t) = \int_0^t \xi_{2t}(t-\tau) k_2 \, e^{-k_2 \tau} \, d\tau, \end{cases} \tag{1}$$

where $k_i$ identifies the streamflow recession rate in the catchment $i$ (i.e., the inverse of the mean response time of the hydrograph). In spite of their simplicity, exponential hydrographs have been successfully employed to characterize streamflow statistics in a wide range of geographical and climatic settings [*Botter et al*., 2007c,; *Pumo et al*., 2013; *Müller and Thompson*, 2015]. The coupling between the dynamics of $q_1$ and $q_2$ emerges from the synchronous effective rainfall events in the two catchments, resulting in the terms $\xi_{1t}$ and $\xi_{2t}$ in equation (1) being correlated.

To investigate the correlation between $q_1$ and $q_2$, it is necessary to introduce some additional parameters that describe the climate forcing within the two contributing catchments. In particular, $\lambda_1$ ($\lambda_2$) identifies the frequency of effective rainfall events that generate streamflow only in the catchment 1 (2) (disjoint events). Conversely, $\lambda_{12}$ identifies the frequency of rainfall events determining a simultaneous streamflow increment in both the outlets (joint events). Because of the low autocorrelation of daily rainfall [*Zorzetto et al*., 2016], joint and disjoint events are assumed as independent Poisson processes. The total frequency of runoff producing events at each catchment outlet is therefore $\lambda_{it} = \lambda_i + \lambda_{12}$. Additionally, let us define the PDF of the intensity of disjoint effective rainfall events in the catchment $i$ as $b_i(h_i)$. Likewise, $b_{12}(h_1, h_2)$ is the bivariate PDF characterizing the depths of effective rainfall when streamflows are simultaneously generated in both catchments (see Table 1 for a detailed list of the notation used in this paper). In summary, the total effective rainfall in equation (1) can be expressed as the sum of two stochastic noises, as detailed below (the first

**Table 1.** Summary of the Parameters

| Parameter | Description |
|---|---|
| $\lambda_{it}$ | Average frequency of all effective rainfall events in catchment $i$ |
| $\lambda_i$ | Average frequency of disjoint effective rainfall events in catchment $i$ |
| $\lambda_{12}$ | Average frequency of joint effective rainfall events in the two catchments |
| $\lambda_m$ | Minimum between $\lambda_{1t}$ and $\lambda_{2t}$ |
| $\alpha_{it}$ | Average depth of all effective rainfall in catchment $i$ |
| $\alpha_i$ | Average depth of disjoint effective rainfall in catchment $i$ |
| $\alpha_i^{12}$ | Average depth of joint effective rainfalls in catchment $i$ |
| $k_i$ | Streamflow decay rate during recessions in catchment $i$ |
| $r_\alpha$ | Correlation between the joint effective rainfall depths in the two catchments |
| $a$ | Slope of the linear relation between the joint effective rainfall depths |
| $b_{it}(h_i)$ | PDF of all effective rainfall depths in catchment $i$ |
| $b_i(h_i)$ | PDF of disjoint effective rainfall depths in catchment $i$ |
| $b_{12}(h_1, h_2)$ | Bivariate PDF of joint effective rainfall depths in the two catchments |
| $b_i^{12}(h_i)$ | Marginal PDF of joint effective rainfall depths in catchment $i$ |
| $\hat{B}_{it}(s_i)$ | Laplace transform of $b_{it}$ |
| $\hat{B}_{12}(s_1, s_2)$ | Laplace transform of $b_{12}$ |

Joint: affects at the same time both catchments; disjoint: affect only one catchment. $i = 1,2$ identifies the two catchments.

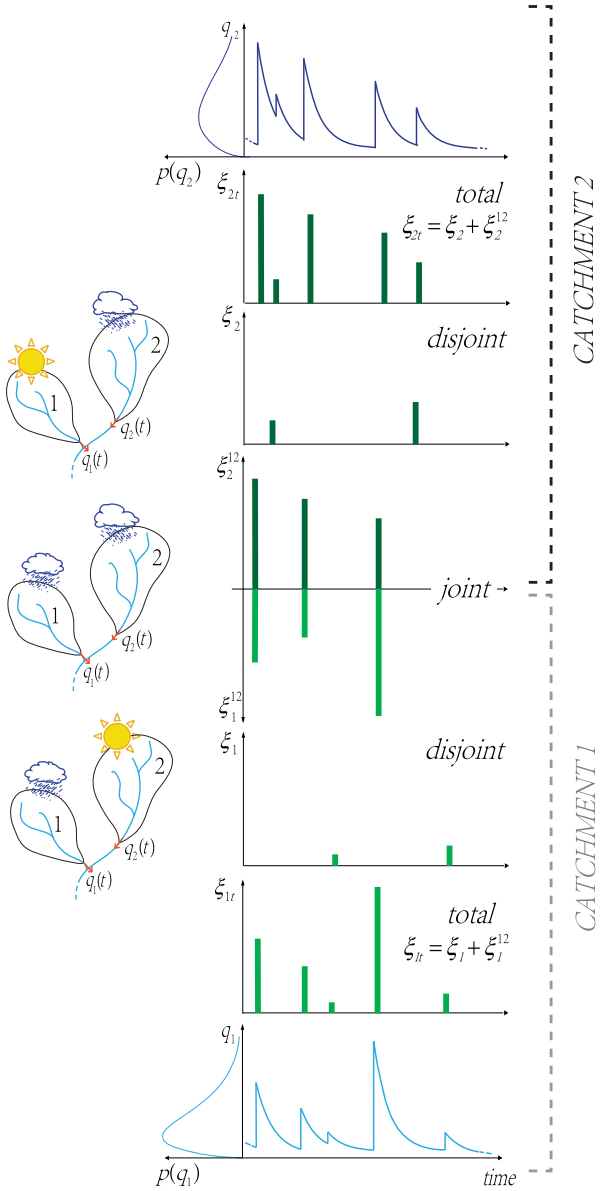


**Figure 2.** When a pair of catchments are simultaneously considered, the overall time series of effective rainfall ($\xi_{it}$) within each catchment can be decoupled into two sub–time series. The first includes the joint effective rainfall events (when streamflow jumps are observed at the outlet of both catchments simultaneously) $\xi_i^{12}$, whereas the other includes the effective rainfall events experienced only by one of the two catchments, $\xi_i$.

argument of each term indicates the average frequency of the effective rainfall events, while the second refers to the PDF of their intensities)

$$\begin{cases} \xi_{1t}[\lambda_{1t};b_{1t}]=\xi_1^{12}\left[\lambda_{12};b_1^{12}\right]+\xi_1[\lambda_1;b_1] \\ \\ \xi_{2t}[\lambda_{2t};b_{2t}]=\xi_2^{12}\left[\lambda_{12};b_2^{12}\right]+\xi_2[\lambda_2;b_2]. \end{cases} \tag{2}$$

The first terms on the right-hand side of equations (2), $\xi_i^{12}$, are related to the streamflow jumps produced by joint effective rainfall events, while the second terms ($\xi_i$) account for the streamflow jumps occurring only at one catchment outlet (disjoint events). In equation (2), the marginal PDF of effective rainfall depths in the catchment $i$ produced by joint events, $b_i^{12}$, can be calculated from the corresponding joint PDF ($b_{12}$) as $b_1^{12}=\int_0^\infty b_{12}(h_1,h_2)\,dh_2$; and $b_2^{12}=\int_0^\infty b_{12}(h_1,h_2)\,dh_1$. Figure 2 graphically represents the decomposition

of the total effective rainfall into joint and disjoint events and the corresponding streamflow dynamics produced at the outlet of each catchment, according to equations (1) and (2). Note that in the proposed formulation, we neglect any kinematic delay between the streamflow jumps observed at the considered catchment outlets in response to joint events. The above simplification is applicable whenever the timescale of flood waves propagation along the river network is shorter than the temporal resolution adopted in this study (1 day). As a rule of thumb, in case of an ideal circular catchment with a maximum channel length equal to its diameter, if we assume a wave celerity of 3 m/s and accept a maximum delay between the hydrograph peaks of 10 hours, the assumption holds for catchment areas $A \lesssim 10^4$ km$^2$.

The master equation for the joint probability density function of the streamflows $q_1$ and $q_2$ associated to equation (1) can be written as [e.g., *Gardiner*, 1983; *Isham et al*., 2005; *Botter et al*., 2008b]:

$$\begin{aligned}\frac{\partial p(q_1,q_2,t)}{\partial t} &= \frac{\partial [k_1 q_1 p(q_1,q_2,t)]}{\partial q_1} + \frac{\partial [k_2 q_2 p(q_1,q_2,t)]}{\partial q_2} + \\ &+ \lambda_1 \int_0^{\frac{q_1}{k_1}} b_1(h_1)\, p(q_1 - k_1 h_1, q_2, t)\, dh_1 + \lambda_2 \int_0^{\frac{q_2}{k_2}} b_2(h_2)\, p(q_1, q_2 - k_2 h_2, t)\, dh_2 + \\ &+ \lambda_{12} \int_0^{\frac{q_1}{k_1}} \int_0^{\frac{q_2}{k_2}} b_{12}(h_1,h_2)\, p(q_1 - k_1 h_1, q_2 - k_2 h_2, t) dh_1 dh_2 - (\lambda_1 + \lambda_2 + \lambda_{12})\, p(q_1,q_2,t).\end{aligned} \tag{3}$$

Equation (3) states that the temporal variation of the joint probability of the streamflows $q_1$ and $q_2$ can be expressed as the sum of six independent terms: the gain/loss of probability due to the deterministic decay of discharge at the outlets 1 and 2 during recessions; the increment of probability due to disjoint streamflow producing events; the increment of probability due to joint streamflow producing events; the loss of probability due to streamflow producing events (regardless of their intensity and nature).

The steady state solution for equation (3) in terms of the moment generating function of the joint PDF of $q_1$ and $q_2$ ($\hat{\hat{p}}(s_1,s_2)$, being $s_1$ and $s_2$ the Laplace variables associated to $q_1$ and $q_2$) reads [e.g., *Van Kampen*, 1992; *Isham et al*., 2005; *Botter et al*., 2007b]

$$\begin{aligned}\hat{\hat{p}}(s_1,s_2) = \exp\Bigg\{ &-\lambda_1 \int_0^\infty \left[1 - \hat{B}_1(k_1 s_1 e^{-k_1 t})\right] dt - \lambda_2 \int_0^\infty \left[1 - \hat{B}_2(k_2 s_2 e^{-k_2 t})\right] dt \\ &- \lambda_{12} \int_0^\infty \left[1 - \hat{\hat{B}}_{12}(k_1 s_1 e^{-k_1 t}, k_2 s_2 e^{-k_2 t})\right] dt \Bigg\},\end{aligned} \tag{4}$$

where $\hat{B}_1$, $\hat{B}_2$, and $\hat{\hat{B}}_{12}$ are the Laplace transforms of $b_1$, $b_2$, and $b_{12}$, respectively.

The correlation between $q_1$ and $q_2$ ($\rho_{12}$) can be derived from equation (4) as detailed in Appendix A. The analytical expression of $\rho_{12}$ reads:

$$\rho_{12} = \frac{\lambda_{12}}{\sqrt{\lambda_{1t}\lambda_{2t}}} \frac{\left. \int_0^\infty \frac{\partial^2 \hat{\hat{B}}_{12}(k_1 s_1 e^{-k_1 t}, k_2 s_2 e^{-k_2 t})}{\partial s_1 \partial s_2} dt \right|_{s_1 = s_2 = 0}}{\sqrt{\left. \int_0^\infty \frac{\partial^2 \hat{B}_{1t}(k_1 s_1 e^{-k_1 t})}{\partial {s_1}^2} dt \int_0^\infty \frac{\partial^2 \hat{B}_{2t}(k_2 s_2 e^{-k_2 t})}{\partial {s_2}^2} dt \right|_{s_1 = s_2 = 0}}}. \tag{5}$$

The analytical expression of the seasonal streamflow correlation (equation (5)) is given by the product between two ratios. The first is related to the frequency of effective rainfall events and it can be interpreted as a normalized frequency of joint events. The second accounts for the intensities of the events as well as for key properties of the hydrologic response in the two contributing catchments (i.e., the rate at which the two basins process the excess of rainfall). It is worth to note that equation (5) holds regardless of the specific distribution chosen for the effective rainfall depths, with the only assumption being that effective rainfall events are homogeneous Poisson processes.

## 3. Exponentially Distributed Effective Rainfall Depths

To make equation (5) operative, the analytical expressions for the PDFs characterizing the effective rainfall depths ($b_{1t}$, $b_{2t}$, and $b_{12}$) need to be defined. In this section we specify equation (5) for exponentially

distributed effective rainfall depths. Exponentially distributed rainfall depths have been frequently employed in analytical studies focused on the impact of stochastic rainfall on the water cycle [*Rodriguez-Iturbe et al*., 1999; *Laio et al*., 2001; *Botter et al*., 2007a, 2008; *Verma et al*., 2011; *Basso et al*., 2015, 2016].

The bivariate distribution $b_{12}(h_1, h_2)$ represents the probability of observing an effective rainfall depth $h_1$ in catchment 1 and an effective rainfall depth $h_2$ in catchment 2 during joint events. The choice of $b_{12}$ is a key point of the analysis because the synchronous increments of discharge (which result from synchronous rainfall events) determine an increase of correlation between the streamflow records at the two outlets (equation (5)). Here $b_{12}$ is assumed to be a bivariate exponential distribution in the form proposed by *Srikanth Iyer et al*. [2001]. This expression has exponential marginals and its parameters are particularly easy to interpret. Moreover, this bivariate PDF allows the description of any positive linear dependence between the variates, yet being parsimonious in terms of the number of parameters. In this case, the analytical expression for the Laplace transform of $b_{12}$, $\hat{\hat{B}}_{12}(s_1, s_2)$, reads [*Srikanth Iyer et al*., 2001]

$$\hat{\hat{B}}_{12}(s_1, s_2) = \left[\frac{1}{1+\alpha_1^{12}(s_1+s_2 a)}\right]\left[\left(1-a\frac{\alpha_1^{12}}{\alpha_2^{12}}\right)\frac{1}{\alpha_2^{12}s_2+1}+a\frac{\alpha_1^{12}}{\alpha_2^{12}}\right], \tag{6}$$

where $\alpha_1^{12}$ and $\alpha_2^{12}$ are the marginal means (the average effective rainfall depths in each catchment produced by joint events) and $a$ is a positive scaling factor that relates the variates by means of the relation: $h_2 = a h_1 + Z$ (where $Z$ is an independent auxiliary random variable, whose distribution modulates the correlation between the two variates). According to equation (6), the correlation between the joint depths $h_1$ and $h_2$ ($r_\alpha$) can be expressed as [*Srikanth Iyer et al*., 2001]:

$$r_\alpha = a\frac{\alpha_1^{12}}{\alpha_2^{12}}. \tag{7}$$

The shape of the bivariate PDF is thus controlled by the parameters $\alpha_1^{12}$, $\alpha_2^{12}$, and $a$ (or, alternatively, by $\alpha_1^{12}$, $\alpha_2^{12}$, and $r_\alpha$). Substituting equation (6) into equation (5), and taking advantage of equation (7), the following expression is obtained:

$$\int_0^\infty \left.\frac{\partial^2 \hat{\hat{B}}_{12}(k_1 s_1 e^{-k_1 t}, k_2 s_2 e^{-k_2 t})}{\partial s_1 \partial s_2}\right|_{s_1=s_2=0} dt = \frac{\alpha_1^{12}\alpha_2^{12}k_1 k_2(1+r_\alpha)}{k_1+k_2}, \tag{8}$$

which will be used to specify the numerator of equation (5).

The solution of equation (5) further requires to specify the overall marginal PDFs of all the effective rainfall depths in the two contributing catchments (including joint and disjoint events) or, alternatively, the PDF of the intensity of the disjoint effective rain depths. For this purpose, exponential univariate distributions have been chosen to preserve consistency with the joint PDF $b_{12}$ given via equation (6). The same assumptions has been done by *Rodriguez-Iturbe et al*. [1999], *Laio et al*. [2001], *Porporato et al*. [2004], *Müller et al*. [2014], and *Dralle et al*. [2016]. Three different cases characterized by a different degree of complexity are presented and discussed in the following. Each of these alternatives can be more or less suited to practical applications depending on data availability and the regional climatology. The first case (section 3.1) represents the simplest model, which assumes that joint and disjoint events are drawn from the same population (i.e., they are characterized by the same depth distribution). The other cases, instead, identify two families of events featured by different statistical properties: joint and disjoint events (Case 2, discussed in section 3.2) or joint and overall events (Case 3, discussed in section 3.3). These models are more complicated and require a larger number of parameters. Case 3, in particular, is consistent with a class of models used for the characterization of flow duration curves [*Botter et al*., 2007a, 2013]. Since there are no theoretical reasons for which one of these models should be preferred a priori, we suggest the model selection should be case specific and performance driven.

### 3.1. Case 1

In this section, the PDF of the overall effective rainfall depths within each catchment is assumed to be equal to the marginal of the bivariate PDF of effective rainfall depths during joint events, i.e., $b_{1t} = b_1^{12}$ and $b_{2t} = b_2^{12}$ (which implies $\hat{B}_{1t}(s_1) = \hat{\hat{B}}_{12}(s_1, 0)$ and $\hat{B}_{2t}(s_2) = \hat{\hat{B}}_{12}(0, s_2)$). Hence, the PDFs describing all the effective rainfall depths within each catchment are exponential distributions with mean $\alpha_i^{12}$. The assumption implies that the distribution

of effective rainfall depths within each catchment is the same for joint and disjoint events. The Laplace transform $\hat{B}_{it}(s_i)$ associated to the PDF of the total effective rainfall depths $b_{it}$ for catchment $i = 1,2$ reads

$$\hat{B}_{it}(s_i) = \frac{1}{1+\alpha_i^{12} s_i}, \tag{9}$$

which leads to

$$\int_0^\infty \frac{\partial^2 \hat{B}_{it}(k_i s_i e^{-k_i t})}{\partial s_i^2} dt \Big|_{s_i=0} = k_i \left(\alpha_i^{12}\right)^2. \tag{10}$$

Combining the result of equations (8) and (10) in equation (5), after some algebra the correlation between $q_1$ and $q_2$ can be written as:

$$\rho_{12} = \frac{\lambda_{12}}{\sqrt{\lambda_{1t}\lambda_{2t}}} \; \frac{1}{2}(1+r_\alpha) \; \frac{2\sqrt{k_1 k_2}}{k_1+k_2}. \tag{11}$$

The structure of equation (11) effectively highlights how different physical processes involved in the underlying streamflow dynamics affect the spatial correlation of streamflows. Three main drivers can be identified: the frequency of effective rainfall; the intensity of effective rainfall; the catchment transport properties. The physical drivers are represented by the three factors $F_\lambda$, $F_\alpha$, and $F_k$ constituting equation (11). Each factor is discussed below.

1. $F_\lambda = \frac{\lambda_{12}}{\sqrt{\lambda_{1t}\lambda_{2t}}}$ (relative frequency of joint streamflow producing rainfall events). This factor represents the relative frequency of synchronous streamflow-producing events (scaled to the geometric mean of the total frequency of events in each catchment). Because $\lambda_{it} = \lambda_{12} + \lambda_i$, the term $F_\lambda$ tends to one when only synchronous events take place. On the other hand, when joint events are not observed in the considered pair of catchments ($\lambda_{12} = 0$), the correlation drops to zero and the streamflow dynamics are uncorrelated, regardless of the other landscape and climate properties.
2. $F_\alpha = \frac{1}{2}(1+r_\alpha)$ (the arithmetic mean between 1 and the correlation of the intensities of the effective rainfall depths during joint events). This factor entails the effect of the correlation between the effective rainfall depths in the two catchments during joint events. Equation (11) shows that the correlation coefficient of the entire streamflow time series is linearly dependent on the correlation between the joint intensities of the effective rainfall in the contributing catchments. However, because of the synchronicity of the joint events and the temporal autocorrelation of the hydrographs, the spatial correlation of streamflow does not drop to zero even for uncorrelated joint depths ($F_\alpha \to 0.5$ when $r_\alpha$ tends to zero). Instead, when the intensity of the joint effective events in the two catchments are highly correlated, $F_\alpha \approx 1$.
3. $F_k = \frac{2\sqrt{k_1 k_2}}{k_1+k_2}$ (ratio between the geometric mean and the arithmetic mean of the recession rates). The last factor accounts for the heterogeneity in the geomorphological and hydrogeological features of the catchments, which result in different timescales of the hydrologic response in the contributing catchments. Note that $F_k \leq 1$, with $F_k = 1$ only when the recession rates in the two catchments are equal.

### 3.2. Case 2

In this case it is assumed that the PDF of the total intensity of the effective rainfall depths is a linear combination of two exponential distributions. The first describes the effective rainfall depths during joint events, while the second refers to the depths of disjoint events. The former is an exponential distribution with mean $\alpha_i^{12}$, while the latter is an exponential distribution with mean $\alpha_i$. The PDF for the total effective rainfall depths within each catchment, $b_{it}$, is a mixed exponential distribution $\left(b_{it} = \frac{\lambda_i}{\lambda_{it}} b_i + \frac{\lambda_{12}}{\lambda_{it}} b_i^{12}\right)$. Accordingly, the Laplace transform $\hat{B}_{it}(s_i)$ of $b_{it}$ can be written as:

$$\hat{B}_{it}(s_i) = \frac{\lambda_i}{\lambda_{it}} \left(\frac{1}{1+\alpha_i s_i}\right) + \frac{\lambda_{12}}{\lambda_{it}} \left(\frac{1}{1+\alpha_i^{12} s_i}\right), \tag{12}$$

which leads to

$$\int_0^\infty \frac{\partial^2 \hat{B}_{it}(k_i s_i e^{-k_i t})}{\partial s_i^2} dt \Big|_{s_i=0} = k_i \frac{\lambda_i (\alpha_i)^2 + \lambda_{12} \left(\alpha_i^{12}\right)^2}{\lambda_{it}}. \tag{13}$$

Inserting equations (8) and (13) into equation (5), the following expression for the spatial correlation of streamflow is obtained:

$$\rho_{12}=\frac{\lambda_{12}\alpha_1^{12}\alpha_2^{12}}{\sqrt{\left[\lambda_1(\alpha_1)^2+\lambda_{12}(\alpha_1^{12})^2\right]\left[\lambda_2(\alpha_2)^2+\lambda_{12}(\alpha_2^{12})^2\right]}}\ \frac{1}{2}(1+r_\alpha)\ \ \frac{2\sqrt{k_1k_2}}{k_1+k_2}. \tag{14}$$

The structure of the above solution is analogous to that of equation (11). However, in equation (14) the frequency and intensity of the effective rainfall are merged in the term $F_{\lambda}^{(2)}=\frac{\lambda_{12}\alpha_1^{12}\alpha_2^{12}}{\sqrt{\left[\lambda_1(\alpha_1)^2+\lambda_{12}(\alpha_1^{12})^2\right]\left[\lambda_2(\alpha_2)^2+\lambda_{12}(\alpha_2^{12})^2\right]}}$ as a consequence of having calculated the overall distributions of the effective rainfall depth based on the relative frequency and intensity of joint and disjoint events (equation (12)). Therefore, in equation (14) the frequencies of the events are weighted based on their mean intensity. Note that since $\lambda_{it}=\lambda_i+\lambda_{12}$, if $\alpha_i=\alpha_i^{12}$, equation (14) turns into equation (11). In fact, equation (11) can be interpreted as a special case of equation (14), corresponding to cases where the depth distributions of joint and disjoint events are equal.

### 3.3. Case 3

In this case it is assumed that, regardless of the shape of $b_{12}$, the overall distributions of the effective rainfall within each catchment ($b_{1t}$ and $b_{2t}$) are exponentials with means $\alpha_{1t}$ and $\alpha_{2t}$. In this case

$$\hat{B}_{it}(s_i)=\frac{1}{1+\alpha_{it}s_i}, \tag{15}$$

which leads to

$$\int_0^\infty \frac{\partial^2\hat{B}_{it}(s_ie^{-k_it})}{\partial {s_i}^2}dt\bigg|_{s_i=0}=k_i\alpha_{it}^2. \tag{16}$$

Combining equations (5), (8), and (16) the following expression for the streamflow correlation is finally obtained

$$\rho_{12}=\frac{\lambda_{12}}{\sqrt{\lambda_{1t}\lambda_{2t}}}\ \ \frac{\alpha_1^{12}\alpha_2^{12}}{\alpha_{1t}\alpha_{2t}}\frac{1}{2}(1+r_\alpha)\ \ \frac{2\sqrt{k_1k_2}}{k_1+k_2}. \tag{17}$$

Equation (17) is similar to equation (11) except for the presence of an additional term related to the effective rain depths ($\frac{\alpha_1^{12}\alpha_2^{12}}{\alpha_{1t}\alpha_{2t}}$). Such term quantifies the ratio between the mean intensities of the joint and the overall effective rainfall events. When $\alpha_i^{12}=\alpha_{it}$ (i.e., the mean depth of joint and total events is the same) equation (17) reduces to equation (11).

## 4. Application

As a proof of concept, we present here an application devoted to test the performances of the model in a real-world setting. To this aim, equation (14) is selected because the statistical differences between the two classes of events (joint and disjoint) are accounted for more explicitly. In equation (14), in fact, the intensity and frequency of joint and disjoint events can be independently specified.

The performances of the analytical model are assessed by comparing the observed correlation of daily flows with the corresponding model estimate for a set of 16 catchments located in the Mid United States (Table 2). The study sites includes all the MOPEX catchments [*Schaake et al*, 2006] within a 120,000 km$^2$ (400 km $\times$ 300 km) region spanning across Arkansas, Missouri, and Oklahoma (http://www.nws.noaa.gov/ohd/mopex/). All basins are weakly impacted by natural or artificial water storages (reservoirs and lakes) and are provided with daily streamflow records from 1948 to 2003. The size of the catchments ranges from 400 to 7500 km$^2$.

From the 16 case studies, 120 combinations of catchment pairs are obtained. The analysis is carried out at seasonal timescale, with seasons defined based on calendar dates (Spring: March, April, May; Summer: June, July, August; Autumn: September, October, November; Winter: December, January, February), leading to

**Table 2.** Summary Information About the Study Catchments

| Number | USGS Code | Name | Area (km$^2$) | Streamflow Gauging Station | State |
|---|---|---|---|---|---|
| 1 | 06928000 | Gasconade River | 3250 | Hazelgreen | MO |
| 2 | 06933500 | Gasconade River | 7384 | Jerome | MO |
| 3 | 07049000 | War Eagle Creek | 684 | Hindsville | AR |
| 4 | 07052500 | James River | 2566 | Galena | MO |
| 5 | 07056000 | Buffalo River | 2155 | St. Joe | AR |
| 6 | 07057500 | North Fork River | 1459 | Tecumseh | MO |
| 7 | 07058000 | Bryant Creek | 1482 | Tecumseh | MO |
| 8 | 07067000 | Current River | 4334 | Van Buren | MO |
| 9 | 07069500 | Spring River | 3068 | Imboden | AR |
| 10 | 07072000 | Eleven Point River | 2938 | Ravenden Springs | AR |
| 11 | 07074000 | Strawberry River | 1230 | Poughkeepsie | AR |
| 12 | 07186000 | Spring River | 3026 | Waco | MO |
| 13 | 07196500 | Illinois River | 2470 | Tahlequah | OK |
| 14 | 07197000 | Baron Fork | 811 | Eldon | OK |
| 15 | 07252000 | Mulberry River | 970 | Mulberry | AR |
| 16 | 07261000 | Cadron Creek | 434 | Guy | AR |

480 couples of seasonal streamflow correlations. For each season, the measured streamflow (Pearson) correlation coefficient between the discharge time series observed at two arbitrary outlets ($\rho_{meas}$) is calculated as

$$\rho_{meas} = \frac{\sum_{i=1}^{n} [(q_1(i) - \langle q_1 \rangle)(q_2(i) - \langle q_2 \rangle)]}{\sqrt{\sum_{i=1}^{n} (q_1(i) - \langle q_1 \rangle)^2 \sum_{i=1}^{n} (q_2(i) - \langle q_2 \rangle)^2}}, \tag{18}$$

where $q_1(i)$ and $q_2(i)$ are the streamflow at the outlet of the catchments 1 and 2 during the $i$-th day, $n$ is the number of recorded days, and $\langle q_1 \rangle$ and $\langle q_2 \rangle$ are the sample averages of $q_1$ and $q_2$.

The model parameters in equation (14) are estimated at seasonal timescale based on observed discharge time series, as discussed below. According to the model formulation, each effective rainfall event produces a discontinuity in the hydrograph (i.e., an abrupt increase of discharge). The frequency of effective rainfall events $\lambda_i$ and $\lambda_{12}$ can therefore be inferred by counting the observed number of jumps in the daily streamflow records at the relevant outlets. These jumps are then classified as "disjoint" or "joint" according to their timing (joint events correspond to synchronous jumps in both catchments). The frequency of joint and disjoint events is then calculated by dividing the number of recorded events for the duration of the considered time series. Similarly, the average effective rainfall intensity, $\alpha$, can be evaluated from the magnitude of the daily streamflow jumps. The depth of each effective rainfall pulse $h_j$ can be computed from the correspondent flow increment $\Delta Q_j$ as $h_j = \frac{\Delta Q_j}{k}$ (see equation (1)). Consequently, $\alpha = \frac{<\Delta Q_j>}{k}$. The analysis is carried out for the different set of streamflow-producing events (joint and disjoint), thereby allowing for the estimate of the corresponding mean depths ($\alpha_i$ and $\alpha_i^{12}$, respectively). In addition, $r_\alpha$ is estimated as the Pearson correlation coefficient between the joint streamflow increments in the two catchments (which are estimated as discussed above). Finally, the recession rate $k$ is evaluated from the observed hydrographs. Since we assume exponential recessions, the drainage rate $k$ is estimated by fitting a linear regression on different pairs $(\frac{\Delta Q}{\Delta t}, Q)$ selected from the descending limbs of observed hydrograph [*Ceola et al.*, 2010; *Basso et al.*, 2015; *Dralle et al.*, 2015].

The model succeeds in reproducing the observed variability of the seasonal streamflow correlation (Figure 3) among the study sites. The scatterplot of Figure 3 shows a good alignment along the 45° line, with a root mean square error $RMSE = 0.086$ and a mean absolute error $MAE = 0.065$. The slight underestimation of the correlation refers to Summer, when reduced discharges are likely to result in less robust estimates of the model parameters.

## 5. Effect of the Spatial Heterogeneity of Hydrologic Properties on the Streamflow Correlation

This section analyzes how the spatial correlation of streamflows is affected by the various parameters involved in the analytical formulation. For this purpose, the solution given via equation (14), which also

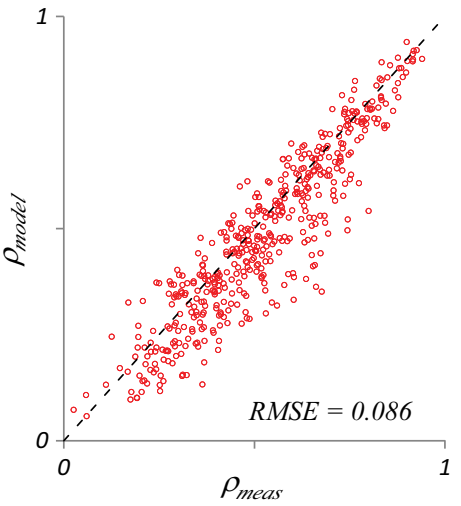


**Figure 3.** The scatterplot shows the performances of the model by comparing the observed and the modeled daily streamflow correlation between all the possible couples of catchment outlets within the study region. The application is performed at seasonal timescale: a single dot represents two catchments during a given season.

includes equation (11) as a special case, is considered. Nevertheless, analogous results can be obtained using the other solution (equations (17)).

The results are discussed in terms of a synthetic dimensionless index, $V \in [0, 1]$, which expresses the inter-catchment variability of climatic and hydrologic properties. For each model parameter we define the corresponding heterogeneity index as $\frac{V(*)=|*_1-*_2|}{*_1+*_2}$, where $*$ represents one of the parameters $\lambda_t$ or $\alpha^{12}$, $k$, and the subscripts 1 and 2 identify the relevant catchments. $V = 0$ implies spatial homogeneity of the considered attribute, while $V = 1$ implies enhanced heterogeneity of the underlying climate/landscape properties.

The analysis is carried out with reference to the three factors of equation (14), namely, $F_\lambda^{(2)}$, $F_\alpha$, and $F_k$. The impact of the heterogeneity of the frequency and intensity of effective rainfall events on the flow correlation is the most difficult to interpret because of the complex structure of $F_\lambda^{(2)}$. Hence, as a first approximation, we shall consider the special case where $\alpha_i = \alpha_i^{12}$, for which $F_\lambda^{(2)} = F_\lambda$ (equation (11)).

Figure 4 (top) shows how the heterogeneity in the frequency of runoff producing events affects the streamflow correlation through the factor $F_\lambda$. The plot shows that such an effect is strongly modulated by the frequency of the joint events $\lambda_{12}$. The decrease of correlation due to the heterogeneity in the frequencies of the overall effective rainfall events $V(\lambda_t)$ is more pronounced for higher frequencies of the joint events. The plot also shows that if $\lambda_{12} < \lambda_m$ ($\lambda_m = \min\{\lambda_{1t}, \lambda_{2t}\}$) there is a potentially significant loss of correlation regardless of the heterogeneity of the overall frequency of effective rainfall events (i.e., for $V(\lambda_t)=0$). Moreover, an additional loss of correlation is observed when $\lambda_{1t} \neq \lambda_{2t}$, which is modulated by the magnitude of $V(\lambda_t)$. It is worth noting that the nested (or non-nested) nature of the catchments directly affects the spatial correlation of flows through the frequency factor $F_\lambda$. In particular, for nested catchments the frequency of joint events shall be equal to the total frequency of the effective rainfall events in the inner catchment (see Figure 5). In fact, the runoff produced from any nested subcatchment of a river propagates along the network and affects the streamflow dynamics downstream, thereby implying that $\lambda_{12} = \lambda_m$ (Figure 5, left). Consequently, the case of nested catchments is described in Figures 4a and 4b by the upper blue lines, which imply larger values of $F_\lambda$ and $\rho_{12}$ for a given value of $V(\lambda_t)$, $V(k)$, $V(\alpha^{12})$, and $a$. Therefore, for a given degree of heterogeneity of climate and landscape attributes, the maximum streamflow correlation is achieved for nested catchments. Conversely, since non-nested catchments are flow-disconnected (Figure 5, right), the frequency of joint runoff events is lower than the minimum frequency of events in each basin. The only exception is the degenerate case where $\lambda_{12} = \lambda_{1t} = \lambda_{2t}$ and $F_\lambda = 1$. The same considerations drawn above concerning the effect of the variability in the frequency of effective rainfall events on $\rho_{12}$ hold in the general case $\alpha_i \neq \alpha_i^{12}$. However, in the latter case there is a significant impact of the ratios $\frac{\alpha_i}{\alpha_i^{12}}$ on the dependence between $\rho_{12}$ and $V(\lambda_t)$ (see Appendix B).

The second factor of equation (14), $F_\alpha = \frac{1}{2}(1+r_\alpha)$, refers to the correlation between the depths of the joint streamflow producing events. In the plots of Figures 4c and 4d the correlation is expressed as a function of $a$ and $V(\alpha^{12})$, as $r_\alpha = a\left(\frac{2}{1-V(\alpha^{12})}-1\right)^{-1}$. As expected, the correlation $\rho_{12}$ decreases with increasing $V(\alpha^{12})$. Though, Figures 4c and 4d show that the sensitivity to $V(\alpha^{12})$ decreases for low values of $a$ and for large values of $V(\alpha_{12})$. Low values of $a$ imply a reduced proportionality between the magnitude of the effective rainfall depths in the two catchments. Hence, for low values of $a$, increasing $V(\alpha^{12})$ does not produce significant impacts on the streamflow correlation.

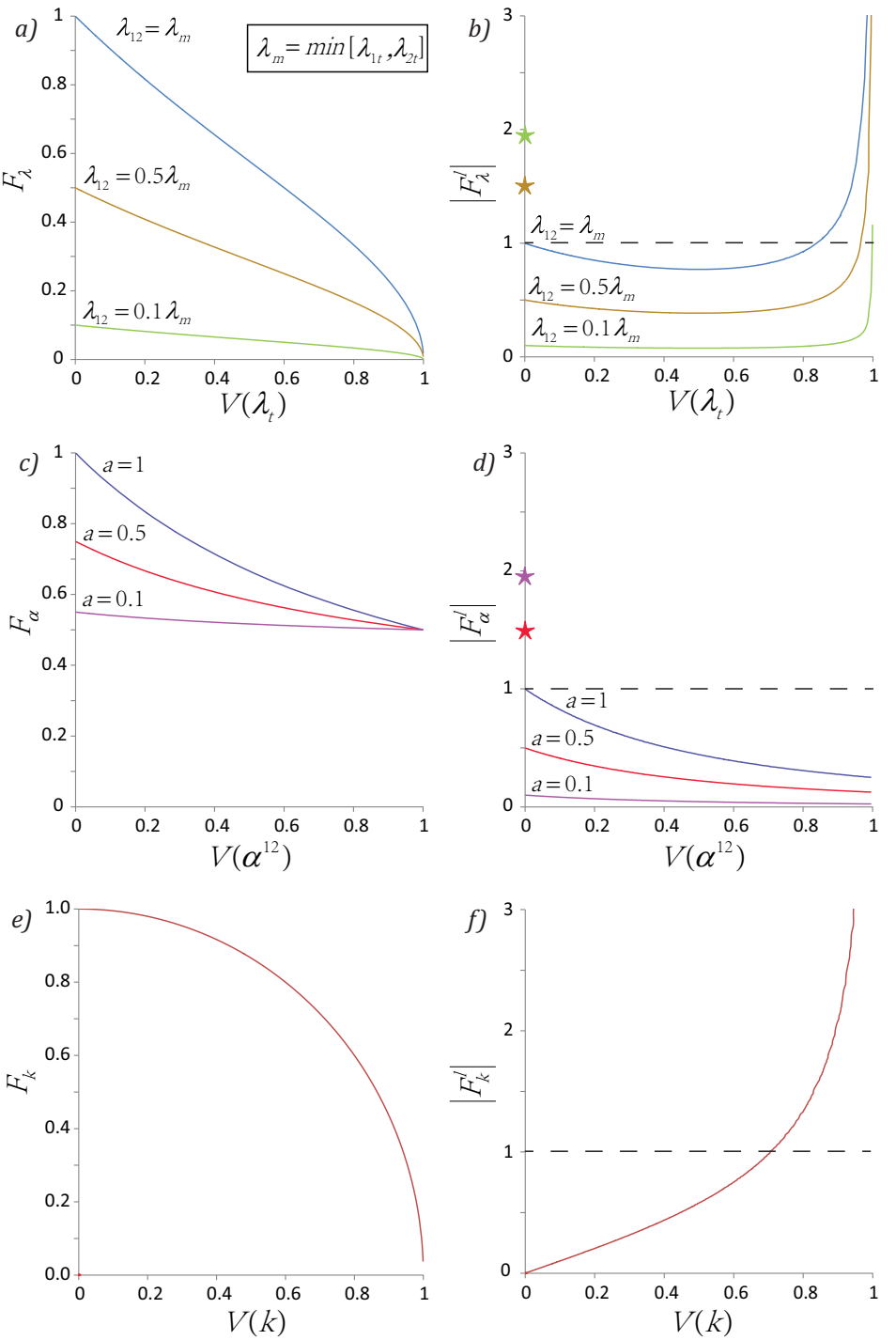


**Figure 4.** The plots show how the three factors in the analytical formulation change as a function of the heterogeneity of the physical parameters involved. The parameters include (i) the average effective rainfall frequencies ($\lambda_{it}$, $\lambda_{12}$); (ii) the average joint effective rainfall depths ($\alpha_i^{12}$) and the correlation $r_\alpha$ between the joint effective rainfall depths (expressed by $a=r_\alpha\frac{\alpha_2^{12}}{\alpha_1^{12}}$); (iii) the streamflow recession rates ($k_i$). The derivative of each factor (right) highlights the sensitivity of $\rho_{12}$ to the heterogeneity of these parameters. In Figures 4c and 4d it is assumed $\alpha_2^{12} > \alpha_1^{12}$. The stars in Figures 4b and 4d indicate step-changes in $F_\lambda$ and $F_\alpha$ (and the $y$ coordinate of each star indicates the relative extent of the corresponding step change).

The factor $F_k=\frac{2\sqrt{k_1k_2}}{k_1+k_2}$ in equation (14) describes how heterogeneity of the response times in the two contributing catchments influence the streamflow correlation at the corresponding outlets. Figures 4e and 4f highlight that the dependence of $F_k$ on $V(k)$ is described by the equation of a circle ($F_k$ is the ratio between the

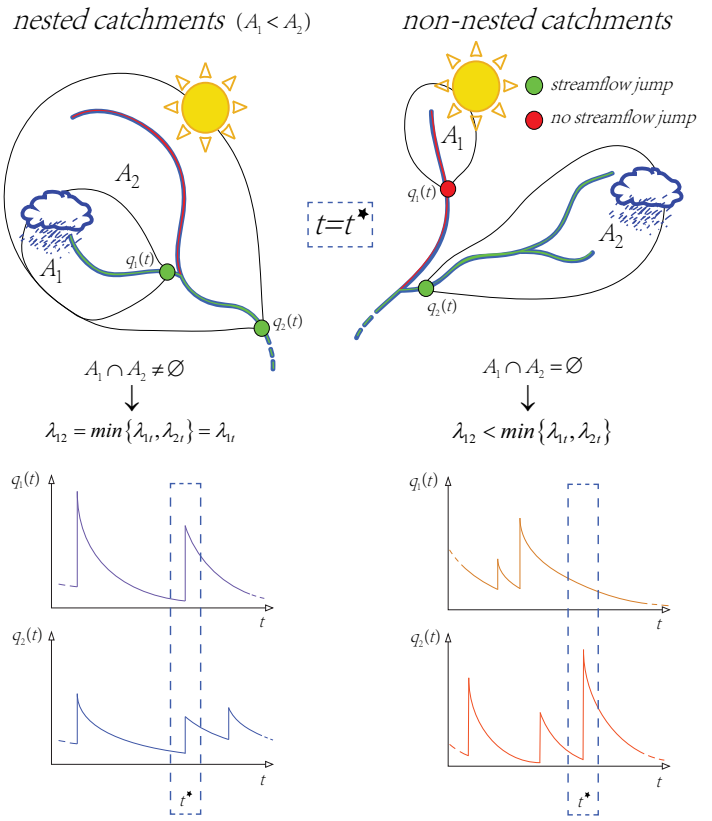


**Figure 5.** Implications of catchment arrangement within a river network for the flow correlation. Two configurations are possible: (i) nested catchments: a smaller catchment ($A_1$) is nested within a larger one ($A_2$); (ii) nonnested catchments: the two catchment areas do not overlap. Due to downstream propagation of streamflows, in case of nested catchments, the frequency of joint runoff events equals the frequency of runoff events in the smaller catchment ($\lambda_{12}=\lambda_{1t}$). In case of non-nested catchments the frequency of joint events is usually smaller than the minimum runoff frequency in the two catchment ($\lambda_{12} < \min\{\lambda_{1t}, \lambda_{2t}\}$).

geometric and the arithmetic mean of the recession parameters). Hence, the correlation coefficient is almost insensitive to small and moderate heterogeneity in the transport properties of the catchments. The impact becomes considerable only for $V(k)\gtrsim 0.6$, which implies that $k_1$ and $k_2$ differ by almost an order of magnitude.

Overall, the analysis suggests that $F_\lambda$ and $F_k$ can independently drive the streamflow correlation to zero. However, the decrease of correlation due to heterogeneity in the frequency of effective rainfall is much larger than that due to differences in the hydrologic response, particularly when the frequency of joint events is relatively small and heterogeneity in recession rates is not exaggerated. Conversely, the heterogeneity in the joint effective rainfall depths described by $F_\alpha$ can decrease correlation by at most a factor of $\frac{1}{2}$. Nevertheless, the influence of the relative intensities of joint and disjoint events on the streamflow correlation should not be underestimated, as discussed in Appendix B.

## 6. Discussion

Despite the simplifications introduced to derive closed-form expressions of the seasonal streamflow correlation, the minimalist model proposed in this paper provides a formal linkage between the spatial correlation of daily flows and the underlying heterogeneity of climate and landscape features. Such a link helps to identify the hierarchy of physical controls acting on the spatial variability of flow regimes, which include the intercatchment variability of precipitation regime, land cover, and recession rates, as well as the topological arrangement of the contributing catchments.

In particular, the theoretical analysis points to the strong influence on the streamflow correlation played by the relative frequency ($\lambda_{12}$) and intensity ($\alpha_i^{12}$) of synchronous effective rainfall events. The analytical model suggests that the occurrence of intense joint flow-producing events in the selected catchments is a major driver of high correlation of streamflow time series. Vice versa: when the frequency of shared events between catchments is low (or the joint events are remarkably less intense than disjoint events), correlation between catchment outflows is also low. Note that the frequency of joint effective rainfall $\lambda_{12}$ encapsulates different climate, soil, and vegetation properties (and their intercatchment variability) according to complex and strongly nonlinear relationships [*Porporato et al.*, 2004; *Isham et al.*, 2005; *Botter et al.*, 2007a; *Doulatyari et al.*, 2014]. In fact, effective rainfall events represent precipitation events that fill the catchment-scale soil moisture deficit created by plant transpiration in the root zone [*Milly*, 1994; *Rodriguez-Iturbe et al.*, 1999; *Laio et al.*, 2001]. As such, the effective rainfall frequency is the by-product of intertwined climate, soil, and vegetation attributes (e.g., rainfall rates, soil storage capacity, and dryness index). Therefore, the presence of synchronous events in the discharge

time series at two selected outlets is influenced by two types of factors: (i) the occurrence of joint rainfall events simultaneously feeding the relevant contributing catchments; (ii) intercatchment similarities of climate/landscape properties like the root zone depth and evapotranspiration rates. In fact, the presence of joint rainfall events is a necessary (though not sufficient) condition to observe high joint frequencies $\lambda_{12}$ (and thus high streamflow correlations). Similarities of landscape attributes also tends to increase the relative frequency of joint flow producing events in the two catchments because of the ensuing similarity in the soil moisture dynamics therein (which implies that the exceedance of the field capacity in the two catchments is more likely triggered by the same rainfall events).

Moreover, it is worth noting that spatial heterogeneity in evapotranspiration and soil properties bears a simultaneous impact both on the frequency of flow-producing events within each catchments ($\lambda_{it}$) and on the frequency of joint events ($\lambda_{12}$), with a potentially limited impact on the factor $F_\lambda = \frac{\lambda_{12}}{\sqrt{\lambda_{1t}\lambda_{2t}}}$ (because of the simultaneous increase/decrease of the total and of the joint frequencies). Instead, since the frequency of joint rainfall events represents a physical upper bound for $\lambda_{12}$, heterogeneity in the rainfall forcing are more directly transmitted to the flow correlation. This instance seems to be an attractive feature of the proposed model, especially in view of possible application to ungauged sites, where $F_\lambda$ could be estimated from spatially interpolated daily precipitation records. As per the depths of effective rainfall, it has been shown elsewhere [e.g., *Rodriguez-Iturbe and Porporato*, 2005] that the main consequence of the interaction between rainfall and soil moisture dynamics is a decrease of the frequency of runoff events, with a more limited impact on the mean depth, at least for exponentially distributed rainfall depths [*Laio et al*., 2001; *Verma et al*., 2011].

Overall, the relative contribution of different climatic and landscape attributes to the streamflow correlation may be dependent on the spatial scales involved in the analysis (e.g., relative distance between catchments, size of the contributing areas) and on the specific climatic setting (e.g., correlation scale of rainfall properties). In small catchments, where climatic features can be expected to be relatively constant over space, small-scale heterogeneity in geological properties, and/or land cover (e.g., presence of karst areas or impervious regions) could significantly enhance the effect of spatially heterogeneous recession rates on the correlation of streamflows. Conversely, in larger catchments located in regions featured by strong climatic gradients (e.g., Alpine or pre-Alpine catchments where orographic effects may enhance the heterogeneity of rainfall) the streamflow correlation should be more strongly related to the spatial variability of rainfall and evapotranspiration. As expected, the topological arrangement of the two outlets also represents a major driver of the spatial correlation of daily flows. In case of nested catchments the correlation tends to increase as a by-product of the following two combined agents: (i) the frequency of joint events equals the minimum frequency of effective rainfall events in the two catchments (i.e., the inner catchment), which increases $\rho_{12}$ as discussed in section 4; (ii) the intercatchment variability of climate, soil, and vegetation properties is reduced (i.e., low values of $V$) because the two relevant contributing areas share a common region of the landscape. This latter effect should be particularly relevant when the two catchments have a similar size.

## 7. Conclusions

In this work we have derived a set of novel analytical expressions for the steady state linear correlation of daily discharges in two arbitrary locations of a river basin at seasonal timescale. The analytical development is based on the assumptions of Poisson effective rainfall and exponential recessions. The time lag between peak hydrographs due to flood wave propagation along the river network is neglected, an instance which may prevent the application of the method to large basins ($A > 10^4$ km$^2$). The resulting expressions for the streamflow correlation involve a limited number of hydrologic parameters that encapsulate soil/vegetation properties, precipitation regime, and recession rates, and correspond to different assumptions on the distribution of effective rainfall depths.

The framework helps to identify the hierarchy of physical controls on the spatial variability of flow regimes. In particular, our theoretical analysis suggests that frequency and intensity of synchronous effective rainfall events in the relevant contributing catchments are the main drivers of the spatial correlation of daily flows, unless the heterogeneity of drainage rates is remarkable. As expected, topological arrangement of the considered outlets also influences the underlying correlation of daily flows. In fact, for nested catchments, the frequency of joint events is equal to the frequency of effective rainfall in the smaller catchment, which implies the maximization

of the spatial correlation of discharge for a given degree of heterogeneity of climate and landscape properties in the two watersheds.

Model performances have been assessed by means of the application of the method to 16 catchments with a maximum size of 7,500 km$^2$ located in a 120,000 km$^2$ region in the United States. The application demonstrated the ability of the model to reproduce the observed streamflow correlations within the study region. Alternative procedures for the estimate of model parameters as well as the comparison among the different solutions in settings where different hydrological data are available are deferred to subsequent studies.

The proposed framework offers the opportunity to improve the characterization of the spatial and temporal variability of flow regimes within and across river basins and it may facilitate the prediction of flow regimes in poorly gauged areas or under changing climate conditions, with implications for water resources assessment and ecological studies.

## Appendix A: Analytical Derivation of the Streamflow Correlation

The spatial correlation of the streamflows at the outlet of two catchments is defined as:

$$\rho_{12}=\frac{cov(q_1,q_2)}{\sqrt{var(q_1)var(q_2)}}, \tag{A1}$$

where $cov(q_1,q_2)=\langle q_1q_2\rangle-\langle q_1\rangle\langle q_2\rangle$ is the streamflows covariance and $\langle q_i\rangle$ indicates the mean flow in catchment $i$. The expectation of the product of the streamfows $\langle q_1q_2\rangle$ can be obtained from the moment generating function (equation (4)) as:

$$\begin{aligned}\langle q_1q_2\rangle&=\frac{d^2\hat{\hat{p}}(s_1,s_2)}{ds_1ds_2}\bigg|_{s_1=0,s_2=0}=\\&=\hat{\hat{p}}(s_1,s_2)|_{s_1=0,s_2=0}\Bigg\{\left[\lambda_1\int_0^\infty\frac{\partial\hat{B}_1(k_1s_1e^{-k_1t})}{\partial s_1}dt+\lambda_{12}\int_0^\infty\frac{\partial\hat{\hat{B}}_{12}(k_1s_1e^{-k_1t},k_2s_2e^{-k_2t})}{\partial s_1}dt\right]\\&\left[\lambda_2\int_0^\infty\frac{\partial\hat{B}_2(k_2s_2e^{-k_2t})}{\partial s_2}dt+\lambda_{12}\int_0^\infty\frac{\partial\hat{\hat{B}}_{12}(k_1s_1e^{-k_1t},k_2s_2e^{-k_2t})}{\partial s_2}dt\right]\\&+\lambda_{12}\int_0^\infty\frac{\partial^2\hat{\hat{B}}_{12}(k_1s_1e^{-k_1t},k_2s_2e^{-k_2t})}{\partial s_1\partial s_2}\,dt\Bigg\}\Bigg|_{s_1=0,s_2=0}.\end{aligned} \tag{A2}$$

The first and the second factors between square brackets on the right-hand side of equation (A2) can be rearranged in terms of the Laplace transform of the "total" probability density function of the jumps, $\hat{B}_{1t}$, which accounts for both joint and disjoint events. In fact, thanks to the independence of joint and disjoint events in equation (2), the overall distribution of the effective rainfall depths, $b_{it}$, can be written as

$$b_{it}=\frac{\lambda_i}{\lambda_{it}}b_i+\frac{\lambda_{12}}{\lambda_{it}}b_i^{12}\qquad(i=1,2). \tag{A3}$$

The Laplace transforms of equation (A3) reads

$$\hat{B}_{1t}(s_1)=\frac{\lambda_1}{\lambda_{1t}}\hat{B}_1(s_1)+\frac{\lambda_{12}}{\lambda_{1t}}\hat{\hat{B}}_{12}(s_1,0)\;\;;\;\;\hat{B}_{2t}(s_2)=\frac{\lambda_2}{\lambda_{2t}}\hat{B}_2(s_2)+\frac{\lambda_{12}}{\lambda_{2t}}\hat{\hat{B}}_{12}(0,s_2), \tag{A4}$$

which allows equation (A2) to be written in terms of $\hat{B}_{1t}$ as:

$$\langle q_1q_2\rangle=\left[\lambda_{1t}\int_0^\infty\frac{\partial\hat{B}_{1t}(k_1s_1e^{-k_1t})}{\partial s_1}dt\right]\left[\lambda_{2t}\int_0^\infty\frac{\partial\hat{B}_{2t}(k_2s_2e^{-k_2t})}{\partial s_2}dt\right]+\lambda_{12}\int_0^\infty\frac{\partial^2\hat{\hat{B}}_{12}(k_1s_1e^{-k_1t},k_2s_2e^{-k_2t})}{\partial s_1\partial s_2}\,dt\bigg|_{s_1=0,s_2=0}. \tag{A5}$$

Similarly, the average streamflow at the outlet of the $i$-th catchment, $\langle q_i\rangle$, can be obtained from the moment generating function of the corresponding marginal streamflow distributions, which can be expressed as [*Kingman*, 1992]:

$$\hat{p}(s_i)=exp\left\{-\lambda_{it}\int_0^{\infty}\left[1-\hat{B}_{it}(k_i s_i e^{-k_i t})\right]dt\right\}. \tag{A6}$$

Equation (A6) leads to the following expression of the expected discharge at the outlet of catchment *i*:

$$\langle q_i\rangle=-\frac{\partial\hat{p}(s_i)}{\partial s_i}\bigg|_{s_i=0}=-\lambda_{it}\int_0^{\infty}\frac{\partial\hat{B}_{it}(k_i s_i e^{-k_i t})}{\partial s_i}dt\bigg|_{s_i=0}. \tag{A7}$$

Combining equations (A5) and (A7), the covariance between the streamflow at the two catchments can then be expressed as:

$$cov(q_1,q_2)=\lambda_{12}\int_0^{\infty}\frac{\partial^2\hat{\hat{B}}_{12}(k_1 s_1 e^{-k_1 t},k_2 s_2 e^{-k_2 t})}{\partial s_1\partial s_2}dt\bigg|_{s_1=s_2=0}. \tag{A8}$$

Equation (A8) states that only joint effective rainfall events generate positive correlations between $q_1$ and $q_2$.

To obtain the final expression of the correlation, the covariance needs to be normalized by means of the product of the standard deviations. To this aim, the streamflow variance at each outlet, $var(q_i)$, is expressed using the moment generating function (equation (A6)) as

$$var(q_i)=\langle q_i^2\rangle-\langle q_i\rangle^2=\frac{\partial^2\hat{p}(s_i)}{\partial s_i{}^2}\bigg|_{s_i=0}-\left[\lambda_{it}\int_0^{\infty}\frac{\partial\hat{B}_{it}(k_i s_i e^{-k_i t})}{\partial s_i}dt\right]^2\bigg|_{s_i=0}=\lambda_{it}\int_0^{\infty}\frac{\partial^2\hat{B}_{it}(k_i s_i e^{-k_i t})}{\partial s_i{}^2}dt\bigg|_{s_i=0}. \tag{A9}$$

Finally, combining equations (A1), (A8), and (A9), the spatial correlation between the streamflows $q_1$ and $q_2$ can be written as in equation (5) of the main text.

## Appendix B: Effect of Heterogeneous Mean Depths of Joint-Disjoint Effective Rainfall Events on $\rho_{12}$

The effect on $\rho_{12}$ due to the frequencies of joint and disjoint events is here assessed in the general case of $\alpha_i \neq \alpha_i^{12}$. In this case, in the factor $F_{\lambda}^{(2)}$ the influence of the frequency of joint and disjoint effective rainfall events is weighted based on their correspondent mean depths.

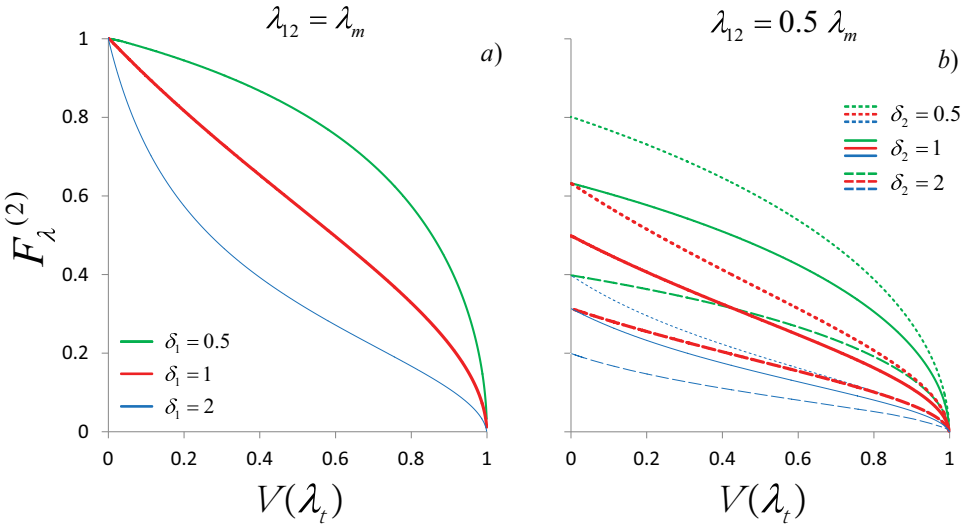


**Figure B1.** Effect of heterogeneous joint and disjoint effective rainfall depths on streamflow correlation for different frequencies of effective rainfall. Differences between joint and disjoint effective rainfall depths within the same catchment *i* are quantified by the ratio $\delta_i=\frac{\alpha_i}{\alpha_i^{12}}$. The couple of ratios $(\delta_1,\delta_2)$ identify each curve. Without loss of generality it is assumed $\lambda_{1t}>\lambda_{2t}$. In Figure B1a the curves are independent on the parameter $\delta_2$ (because $\lambda_2=0$). The solid red curve corresponds to equation (11) and Figure 4. As defined in the text, $\lambda_m=\min\{\lambda_{1t},\lambda_{2t}\}$.

Figure B1 shows how $F_{\lambda}^{(2)}$ (and hence the correlation $\rho_{12}$) decreases as a function of $V(\lambda_t)$ for different frequencies $\lambda_{12}$ and different combinations of the spatial heterogeneity between the mean intensity of joint and disjoint events. The latter is quantified by means of ratios $\delta_i = \frac{\alpha_i}{\alpha_{12}}$. Figure B1 shows how the ratio $\delta_1$ modulates the dependence of $F_{\lambda}^{(2)}$ on $V(\lambda_t)$ when $\lambda_{12} = \lambda_m$ (which implies $\lambda_2 = 0$). When $\delta_1 < 1$ (high relative intensity of joint events), the effect of joint effective rainfalls is enhanced and high values of $F_{\lambda}^{(2)}$ are maintained for a wide range of $V(\lambda_t)$. Conversely, high values of $\delta_1$ ensue a faster loss of correlation, despite relatively high frequency of joint events (low values of $V(\lambda_t)$).

In Figure B1 the effect of $\delta_i$ is assessed in the case $\lambda_{12} = 0.5\,\lambda_m$. In this case the heterogeneity of the intensities affects $F_{\lambda}^{(2)}$ also when $V(\lambda_t) = 0$. Higher values of correlation are ensured by low values of $\delta_i$. On the contrary, a significant drop of correlation is observed when the intensities of disjoint events are high compared to the intensities of joint events (i.e., for higher values of $\delta_i$).

This analysis pinpoints the intertwined role of the frequency and intensity of effective rainfall events on the streamflow correlation. In particular, heterogeneity in the relative mean depths between joint and disjoint effective rainfall can strongly impact the dependence of $F_{\lambda}^{(2)}$ on $V(\lambda_t)$.

**Acknowledgments**

This project has received funding from the European Union's Horizon 2020 research and innovation program under the Marie Sklodowska-Curie grant 641939. This study was also funded by the Swiss National Science Foundation (SNF project 200021-149126). Additional support was provided by the Competence Center Environment and Sustainability (CCES) of the ETH domain in the framework of the RECORD Catchment project. All the hydrologic data used in this study are taken from the MOPEX data set and are freely available online at http://www.nws.noaa.gov/ohd/mopex/. The authors would like to thank the three anonymous reviewers and the Associate Editor for having contributed to improve the quality of this work with their comments.

## References

Andres-Domenech, I., R. Garcia-Bartual, A. Montanari, and J. B. Marco (2015), Climate and hydrological variability: The catchment filtering role, *Hydrol. Earth Syst. Sci.*, *19*, 379–387, doi:10.5194/hess-19-379-2015.

Archfield, S. A., and R. M. Vogel (2010), Map correlation method: Selection of a reference streamgage to estimate daily streamflow at ungaged catchments, *Water Resour. Res.*, *46*, W10513, doi:110.1029/2009WR008481.

Basso, S., A. Frascati, M. Marani, M. Schirmer, and G. Botter (2015), Climatic and landscape controls on effective discharge, *Geophys. Res. Lett.*, *42*, 8441–8447, doi:10.1002/2015GL066014.

Basso, S., M. Schirmer, and G. Botter (2016), A physically based analytical model of flood frequency curves, *Geophys. Res. Lett.*, *43*, 9070–9076, doi:10.1002/2016GL069915.

Blöschl, G. (2006), Rainfall-runoff modeling of ungauged catchments, *Encycl. Hydrol. Sci.*, *11*, 133, doi:10.1002/0470848944.hsa140.

Blöschl, G., M. Sivapalan, T. Wagener, A. Viglione, and H. Savenije (2013), *Runoff Prediction in Ungauged Basins: Synthesis across Processes, Places and Scales*, Cambridge Univ. Press, Cambridge.

Botter, G., A. Porporato, I. Rodriguez-Iturbe, and A. Rinaldo (2007a), Basin-scale soil moisture dynamics and the probabilistic characterization of carrier hydrologic flows: Slow, leaching-prone components of the hydrologic response, *Water Resour. Res.*, *43*, W02417, doi:10.1029/2006WR005043.

Botter, G., A. Porporato, E. Daly, I. Rodriguez-Iturbe, and A. Rinaldo (2007b), Probabilistic characterization of base flows in river basins: Roles of soil, vegetation, and geomorphology, *Water Resour. Res.*, *43*, W06404 doi:10.1029/2006WR005397.

Botter, G., F. Peratoner, A. Porporato, I. Rodriguez-Iturbe, and A. Rinaldo (2007c), Signatures of large-scale soil moisture dynamics on streamflow statistics across U.S. climate regimes, *Water Resour. Res.*, *43*, W11413, doi:10.1029/2007WR006162.

Botter, G., S. Zanardo, A. Porporato, I. Rodriguez-Iturbe, and A. Rinaldo (2008a), Ecohydrological model of flow duration curves and annual minima, *Water Resour. Res.*, *44*, W08418, doi:10.1029/2008WR006814.

Botter, G., E. Daly, A. Porporato, I. Rodriguez-Iturbe, and A. Rinaldo (2008b), Probabilistic dynamics of soil nitrate: Coupling of ecohydrological and biogeochemical processes, *Water Resour. Res.*, *44*, W03416, doi:10.1029/2007WR006108.

Botter, G., S. Basso, I. Rodriguez-Iturbe, and A. Rinaldo (2013), Resilience of river flow regimes, *Proc. Natl. Acad. Sci. U. S. A.*, *110*, 12,925–12,930, doi:10.1073/pnas.1311920110.

Castellarin, A., G. Galeati, L. Brandimarte, A. Montanari, and A. Brath (2004), Regional flow-duration curves: Reliability for ungauged basins, *Adv. Water Resour.*, *27*, 953–965, doi:10.1016/j.advwatres.2004.08.005.

Castellarin, A., G. Camorani, and A. Brath (2007), Predicting annual and long-term flow-duration curves in ungauged basins, *Adv. Water Resour.*, *30*, 937–953, doi:10.1016/j.advwatres.2006.08.006.

Castiglioni, S., I. Lombardi, E. Toth, A. Castellarin, and A. Montanari (2010), Calibration of rainfall-runoff models in ungauged basins: Regional maximum likelihood approach, *Adv. Water Resour.*, *33*, 1235–1242, doi:10.1016/j.advwatres.2010.04.009.

Castiglioni, S., A. Castellarin, A. Montanari, J. O. Skøjen, G. Laaha, and G. Blöschl (2011), Smooth regional estimation of low-flow indices: Physiographical space based interpolation and top-kriging, *Hydrol. Earth Syst. Sci.*, *15*, 715–727, doi:10.5194/hess-15-715-2011.

Ceola, S., G. Botter, E. Bertuzzo, A. Porporato, I. Rodriguez-Iturbe, and A. Rinaldo (2010), Comparative study of ecohydrological streamflow probability distributions, *Water Resour. Res.*, *46*, W09502, doi:10.1029/2010WR009102.

Cheng, L., M. Yaeger, A. Viglione, E. Coopersmith, S. Ye, and M. Sivapalan (2012), Exploring the physical controls of regional patterns of flow duration curves Part 1: Insights from statistical analyses, *Hydrol. Earth Syst. Sci.*, *16*, 4435–4446, doi:10.5194/hess-16-4435-2012.

Claps, P., A. Giordano, and F. Laio (2005), Advances in shot noise modeling of daily streamflows, *Adv. Water Resour.*, *28*, 992–1000, doi:10.1016/j.advwatres.2005.03.008.

Costa-Cabral, M. C., J. E. Richey, G. Goteti, D. P. Lettenmaier, C. Feldkteer, and A. Snidvongs (2008), Landscape structure and use, climate, and water movement in the Mekong River basin, *Hydrol. Processes*, *22*, 1731–1746, doi:10.1002/hyp.6740.

Doulatyari, B., S. Basso, M. Schirmer, and G. Botter (2014), River flow regimes and vegetation dynamics along a river transect, *Adv. Water Resour.*, *73*, 30–43, doi:10.1016/j.advwatres.2014.06.015.

Doulatyari, B., A. Betterle, S. Basso, B. Biswal, M. Schirmer, and G. Botter (2015), Predicting streamflow distributions and flow duration curves from landscape and climate, *Adv. Water Resour.*, *83*, 285–298, doi:10.1016/j.advwatres.2015.06.013.

Dralle, D., N. Karst, and S. Thompson (2015), a, b careful: The challenge of scale invariance for comparative analyses in power law models of the streamflow recession, *Geophys. Res. Lett.*, *42*, 9285–9293, doi:10.1002/2015GL066007.

Dralle, D., N. Karst, and S. Thompson (2016), Dry season streamflow persistence in seasonal climates, *Water Resour. Res.*, *52*, 90–107, doi:10.1002/2015WR017752.

Gardiner, C. W. (1983), *Handbook of Stochastic Methods*, Springer, Berlin.

Hirsch, R. M. (1982), A comparison of four streamflow record extension techniques, *Water Resour. Res.*, *18*, 1081–1088, doi:10.1029/WR018i004p01081.
Hurford, A. P., and J. J. Harou (2014), Balancing ecosystem services with energy and food security-assessing trade-offs from reservoir operation and irrigation investments in Kenya's Tana Basin, *Hydrol. Earth Syst. Sci.*, *18*, 3259–3277, doi:10.5194/hess-18-3259-2014.
Isham, V., D. Cox, I. Rodriguez-Iturbe, A. Porporato, and S. Manfreda (2005), Representation of space time variability of soil moisture, *Proc. R. Soc. A*, *461*(2064), 4035–4055, doi:10.1098/rspa.2005.1568.
Kiang, J. E., D. W. Stewart, S. A. Archfield, E. B. Osborne, and K. Eng (2013), A national streamflow network gap analysis, *U.S. Geol. Surv. Sci. Invest. Rep., 2013-5013*, 79 pp.
Kingman, J. F. C. (1992), *Poisson Processes*, Oxford Univ. Press, Clarendon, Oxford.
Kollet, S., and R. Maxwell (2008), Capturing the influence of groundwater dynamics on land surface processes using an integrated, distributed watershed model, *Water Resour. Res.*, *44*, W02402, doi:10.1029/2007WR006004.
Lahaa, G., J. O. Skøjen, and G. Blöschl (2014), Spatial prediction on river networks: Comparison of top-kriging with regional regression, *Hydrol. Processes*, *28*, 315–324, doi:10.1002/hyp.9578.
Laio, F., A. Porporato, L. Ridolfi, and I. Rodriguez-Iturbe (2001), Plants in water-controlled ecosystems: Active role in hydrologic processes and response to water stress, II. *Probabilistic soil moisture dynamics, Adv. Water Resour.*, *24*, 707–723, doi:10.1016/S0309-1708(01)00005-7.
Messinger, T., and K. S. Paybins (2014), Correlations of daily flows at streamgages in and near West Virginia, 1930-2011, and streamflow characteristics relevant to the use of index streamgages, *U.S. Geol. Soc. Sci. Invest. Rep.*, *2014-5061*, 83 pp., doi:10.3133/sir20145061.
Milly, P. C. D. (1994), Climate, soil water storage, and the average annual water balance, *Water Resour. Res.*, *30*(7), 2143–2156, doi:10.1029/94WR00586.
Mc Guire, K., C. Torgersen, G. Likens, D. Buso, W. Lowe, and S. Bailey (2014), Network analysis reveals multiscale controls on streamwater chemistry, *Proc. Natl. Acad. Sci. U. S. A.*, *111*, 7030–7035, doi:10.1073/pnas.1404820111.
Müller, M. F., D. N. Dralle, and S. E. Thompson (2014), Analytical model for flow duration curves in seasonally dry climates, *Water Resour. Res.*, *50*, 5510–5531, doi:10.1002/2014WR015301.
Müller, M. F., and S. E. Thompson (2015), Stochastic or statistic? Comparing flow duration curve models in ungauged basins and changing climates, *Hydrol. Earth Syst. Sci. Discuss.*, *20*, 669–683, doi:10.5194/hessd-12-9765-2015.
Porporato, A., E. Daly, and I. Rodriguez-Iturbe (2004), Soil water balance and ecosystem response to climate change, *Am. Nat.*, *164*, 625–632, doi:10.1086/424970.
Postel, S., and B. Richter (2003), *Rivers for Life: Managing Water for People and Nature*, Island Press, Washington, D. C., doi:10.1002/rra.820.
Pumo, D., L. V. Noto, and F. Viola (2013), Ecohydrological modelling of flow duration curve in Mediterranean river basins, *Adv. Water Resour.*, *52*, 314–327, doi:10.1016/j.advwatres.2012.05.010.
Rigon, R., G. Bertoldi, and T. M. Over (2006), GEOtop: A distributed hydrological model with coupled water and energy budgets, *J. Hydrometeorol.*, *7*, 371–388, doi:10.1175/JHM497.1.
Rodriguez-Iturbe, I., A. Porporato, L. Ridolfi, V. Isham, and D. R. Coxi (1999), Probabilistic modelling of water balance at a point: The role of climate, soil and vegetation, *Proc. R. Soc. A*, *455*(1990), 3789–3805, doi:10.1098/rspa.1999.0477.
Rodriguez-Iturbe, I., and A. Porporato (2005), *Ecohydrology of Water-Controlled Ecosystems: Soil Moisture and Plant Dynamics*, Cambridge Univ. Press, Cambridge.
Schaake, J., S. Cong, and Q. Duan (2006), *U.S. MOPEX Data Set*, *IAHS Publ. Ser*, *307*, 9–28.
Schaefli, B., L. Nicotina, C. Imfeld, P. Da Ronco, E. Bertuzzo, and A. Rinaldo (2014), Spatially explicit hydrologic response model for ecohydrologic applications, *Geosci. Model Dev.*, *7*, 2733–2746, doi:10.5194/gmd-7-2733-2014.
Sivakumar, B., and F. M. Woldemeskel (2014), Complex networks for streamflow dynamics, *Hydrol. Earth Syst. Sci.*, doi:10.5194/hess-18-4565-2014.
Skøjen, J. O., R. Merz, and G. Blöschl (2006), Top-kriging geostatistics on stream networks, *Hydrol. Earth Syst. Sci.*, *10*, 277–287, doi:10.5194/hess-10-277-2006.
Srikanth Iyer, K., D. Manjunath, and R. Manivasakan (2001), Bivariate exponential distributions using linear structures, *Indian J. Stat. Ser. A*, *64*(1), 156–166.
Thompson, S. E., C. J. Harman, A. G. Konings, M. Sivapalan, A. Neal, and P. A. Troch (2011), Comparative hydrology across AmeriFlux sites: The variable roles of climate, vegetation, and groundwater, *Water Resour. Res.*, *47*, W00J07, doi:10.1029/2010WR009797.
Van Kampen, N. G. (1992), *Stochastic Processes in Physics and Chemistry*, Elsevier, New York.
Verma, P., J. Yeates, and E. Daly (2011), A stochastic model describing the impact of daily rainfall depth distribution on the soil water balance, *Adv. Water Resour.*, *34*, 1039–1048, doi:10.1016/j.advwatres.2011.05.013.
Vogel, R. M., and J. R. Stedinger (1985), Minimum variance streamflow record augmentation procedures, *Adv. Water Resour.*, *21*(5), 715–723, doi:10.1029/WR021i005p00715.
Zehe, E., and G. Blöschl (2004), Predictability of hydrologic response at the plot and catchment scales: Role of initial conditions, *Water Resour. Res.*, *40*, W10202, doi:10.1029/2003WR002869.
Ziv, G., E. Baran, S. Nam, I. Rodriguez-Iturge, and S. Levin (2012), Trading-off fish biodiversity, food security and hydropower in the Mekong river basin, *Proc. Natl. Acad. Sci. U. S. A.*, *109*, 5609–5614, doi:10.1073/pnas.1201423109.
Zorzetto, E., G. Botter, and M. Marani (2016), On the emergence of rainfall extremes from ordinary events, *Geophys. Res. Lett.*, *43*, 8076–8082, doi:10.1002/2016GL069445.